Weighted Harmonic and Ginzburg-Landau equations in image inpainting

Zakaria Belhachmi, Moez Kallel, Maher Moakher, Anis Theljani

Weighted Harmonic and Ginzburg-Landau equations in image inpainting

Zakaria BELHACHMI *, Moez KALLEL†, Maher MOAKHER †, and Anis THELJANI †*
†ENIT-LAMSIN, University of Tunis El Manar, Tunisia.
*Mathematics, Information Technology and Applications Laboratory, University of Haute Alsace, France.
‡Emails: zakaria.belhachmi@uha.fr moez.kallel@ipeit.rnu.tn maher.moakher@enit.rnu.tn thaljanianis@gmail.com

***Abstract*—We consider some second-order variational model for solving image inpainting problems. The aim is to obtain as far as possible fine features of the initial image, e.g. corners, edges, ...in the inpainted region. The approach consists of constructing a family of regularized functionals and to select locally and adaptively the regularization parameters with a posteriori error indicators. The parameters selection is performed at the discrete level in the framework of the finite element method. We present several numerical simulations to test the efficiency of the proposed approach.**

INTRODUCTION

Image inpainting or disocclusion refers to restoring a damaged image with missing information. This type of image processing treatment is very important and it has many applications in various fields (painted canvas and movies restoration, augmented reality, ...). In fact, many images are often scratched and damaged, the goal of image inpainting is to restore the deteriorated parts, in such a manner, that a viewer can not detect these parts. Different techniques are applied to solve this problem, in particular, Partial Differential Equations (PDEs) are widely used and are proven to be efficient ([1], [2], [3], [4]). A number of PDE based approaches inpainting were introduced in the literature. They can be classified into linear or nonlinear, isotropic or anisotropic equation. The major drawback of the linear ones is that they have a strong smoothing effect. They fail to inpaint images with edges (discontinuities). Therefore, nonlinear models were used in order to overcome this strong regularization effect and to preserve the contours (edges) across the region to be inpainted. Without being exhaustive, we refer to [1], [2], [3] for the image inpainting problem.

We consider in this work a novel approach which consists of an adaptive method for PDE models in image inpainting. This approach is well suited to obtain fine features of the initial (damaged) image , e.g. edges, corners, ... although the used continuous model is formally linear. Loosely speaking, we start with a simple model (e.g. linear diffusion with a variable coefficient), the method consists of choosing locally and adaptively the values of diffusion coefficient with the help of some informations on the gradient magnitude. The informations are available at the discrete level from the computed solution, thus the process is completely a posteriori-based parameter selection. This approach was introduced by Hecht and Belhachmi in [5] and [6] for optic flow estimation, where it was demonstrated to have several attractive features such as: the efficiency (e.g. cost of computation, best representation of the solution,...) as well as a good edge-preserving ability. Moreover, it was proven in [6] that this approach allows to approximate, in the Γ-convergence sense [7], the well known Mumford-Shah functional (see [8], [9]) although formally the continuous model is linear.

I. WEIGHTED HARMONIC INPAINTING

We consider a planar image u defined in a domain $\Omega \subset R^2$, usually a rectangular domain with piecewise smooth boundary $\partial\Omega$. $D \subset \Omega$ is a sub-domain in Ω, as shown in Fig. 1. We

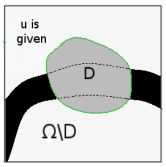

Fig. 1. Image domain

assume that u is contaminated by a Gaussian white noise n in $\Omega\backslash D$ and that its restriction in D was distorted. The goal of the Harmonic inpainting [1] is to find a function $u \in H^1(\Omega)$ that minimizes the following energy functional:

$$F(u) = \frac{1}{2}\int_\Omega |\nabla u|^2 dx + \int_\Omega \frac{\lambda(x)}{2}(u-f)^2 dx, \qquad (1)$$

where $\lambda = \lambda_0$ in $\Omega\backslash D$ (Full attachment outside inpainting area) and 0 in D (No attachment to the input image f within inpainting area). The first part of (1) encodes the image model (diffusion term) and the second is called the fidelity part. The Euler-Lagrange equation for the energy functional F is

$$\begin{cases} -\Delta u + \lambda(u-f) = 0, & \text{in } \Omega, \\ \partial_n u = 0, & \text{on } \partial\Omega, \end{cases} \qquad (2)$$

It is an isotropic linear diffusion PDE and it is unable to restore narrow broken edges due to its strong regularization effects. While, edges are crucial for object recognition in image processing problems. We then introduce an adaptive strategy which can restore edges whilethe continos model belonging (formally) to the linear diffusion class of methods. We consider the following minimization problem:

$$\min_{u_\alpha \in H^1(\Omega)} F_\alpha(u_\alpha), \qquad (3)$$

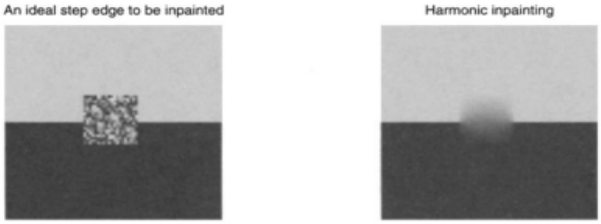

Fig. 2. Example of Harmonic inpainting (T. Chan and J. Shen [1])

where

$$F_\alpha(u) = \frac{1}{2}\int_\Omega \alpha(x)|\nabla u|^2 dx + \int_\Omega \frac{\lambda(x)}{2}(u-f)^2 dx.$$

We assume that the lifting parameter α is given, scalar, piecewise constant function on Ω. The domain Ω is partitioned into a "n" disjoint finite number of sub-domains Ω_l such that

$$\alpha = \alpha_l \; in \; \Omega_l \;\; 1 \leq l \leq n$$

We denote $\alpha_m = \min_{1\leq l\leq n} \alpha_l$, respectively $\alpha_M = \max_{1\leq l\leq n} \alpha_l$, and we assume that $\alpha_m > 0$.

Proposition 1: Let $f \in L^2(\Omega)$ be given such that $|f(x)| \leq 1$ a.e. in Ω. The minimization problem (3) admits a unique minimizer u_α in $H^1(\Omega)$ with $|u_\alpha(x)| \leq 1$ a.e. in Ω.
The minimizer u_α of (3) verifies the following Euler-Lagrange equation:

$$\begin{cases} -\nabla.(\alpha(x)\nabla u_\alpha) + \lambda(u_\alpha - f) = 0, & \text{in } \Omega, \\ \partial_n u_\alpha = 0, & \text{on } \partial\Omega, \end{cases} \tag{4}$$

The parameters selection strategy is performed at the discrete level in the framework of the finite element method (i. e., weak solution). Therefore, we define the following variational formulation:

$$\begin{cases} \text{find } u_\alpha \in H^1(\Omega), \text{ such that} \\ \int_\Omega \alpha(x)\nabla u \cdot \nabla v dx + \int_\Omega \lambda uv dx = \int_\Omega \lambda f v dx, \; \forall v \in H^1(\Omega), \end{cases} \tag{5}$$

The equivalence of the problems (5) and (3) follows by standard arguments. Noting that for $|u(x)| \leq 1$ in Ω and for $\alpha_m > 0$, the ellipticity of the bilinear form $a_\alpha(.,.)$ in the space $H^1(\Omega)$ is immediate.

A. Discrete problem and adaptivity

We assume that the domain Ω is polygonal. We consider a regular family of triangulations $\mathcal{T}_h$ made of elements which are triangles (or quadrilaterals) with a maximum size h, satisfying the usual admissibility assumptions, i.e., the intersection of two different elements is either empty, a vertex, or a whole edge. For $h > 0$, we introduce the following discrete space:

$$X_h = \left\{ v_h \in C(\overline{\Omega}) | \forall K \in \mathcal{T}_h, v_h|_K \in P_1(K) \right\},$$

The discrete problem leads to:

$$\begin{cases} \text{find } u_{\alpha,h} \in H^1(\Omega), \text{ such that} \\ \int_\Omega \alpha_h \nabla u_h \cdot \nabla v_h dx + \int_\Omega \lambda u_h v_h dx = \int_\Omega \lambda f_h v_h dx, \; \forall v_h \in H^1(\Omega), \end{cases} \tag{6}$$

where f_h is a finite element approximation of f associated with $\mathcal{T}_h$. Applying the Lax-Milgram Lemma, we can prove that there exists a unique solution $u_{\alpha,h}$ in $H^1(\Omega)$ of the discrete problem (6) with $|u_{\alpha,h}(x)| \leq 1$ a.e. in Ω.

II. Adaptive local choice of α

For an element $K \in \mathcal{T}_h$, we denote by E_K the set of its edges not contained in the boundary $\partial\Omega$. The union of all E_K, $K \in \mathcal{T}_h$ is denoted by E_h. With each edge $e \in E_h$, we associate a unit vector n_e normal to e and we denote by $[\phi]_e$ the jump of the piecewise continuous function ϕ across e in the direction n_e. For each $K \in \mathcal{T}_h$, we denote by h_K the diameter of K and we denote by h_e the length of e, $e \in E_K$ and f_h a finite element approximation of f. We define the residual error indicator as follows: for each element $K \in \mathcal{T}_h$, we set:

$$\eta_K^1 = \alpha_K^{-\frac{1}{2}} h_K ||\lambda(u_{\alpha,h} - f_h) + \alpha_h \Delta u_{\alpha,h}||_{L^2(K)} + \tfrac{1}{2} \sum_{e\in E_K} \alpha_e^{-\frac{t}{2}} h_e^{\frac{1}{2}} |||[\alpha \nabla u_{\alpha,h} \cdot n_e]||_{L^2(e)}$$

where $\alpha_e = \max(\alpha_{K1}, \alpha_{K2})$, K_1 and K_2 being the two elements adjacent to e.
On the triangulation $\mathcal{T}_h$, we compute the solution $u_{\alpha,h}$ of problem (6) and the corresponding error indicator which is well known to be equivalent to the H^1-norm of the finite element error (see [10] for details) and allows mostly mesh adaptation. Although η_K^1 is standard information on the error distribution of the computations of $u_{\alpha,h}$, it encodes some priory information about edges in the following term

$$\tfrac{1}{2} \sum_{e\in E_K} \alpha_e^{-\frac{1}{2}} h_e^{\frac{1}{2}} |||[\alpha \nabla u_{\alpha,h} \cdot n_e]||_{L^2(e)}. \tag{7}$$

In fact, the edges in the image are characterized by regions when the brightness changes sharply (large gradients) or, more formally, has discontinuities. Therefore, the quantity (7) acts as a measure locating regions of edges and will be used next to control and to select the parameter α.

Remark 1: Since all error indicators are mainly equivalent [10], we can change the error indicator η_K^1 by the following local energy

$$\eta_K^2 = \alpha_K^{\frac{1}{2}} ||\nabla u_{\alpha,h}||_{L^2(K)} \tag{8}$$

which might be well suited in the adaptation steps and behaves more or less like the residual error indicator when we use P_1 Lagrange finite elements.

1) **Adaptive strategy***:* We control the diffusion process by the following adaptive algorithm: Given the grid $\mathcal{T}_h^0$ corresponding to the image, we:

1) Compute $u_{\alpha^0,h}$ solution of the problem (4) on $\mathcal{T}_h^0$ with a large constant $\alpha = \alpha^0$.
2) We build an adapted isotropic mesh $\mathcal{T}_h^1$ with the error indicator η_K^i $i = 1, 2$).
3) We perform an automatic local choice of $\alpha(x)$ on $\mathcal{T}_h^1$ to obtain a new function $\alpha_1(x)$ in D.
4) Go to steps (2) and (3) and compute $u_{\alpha_1,h}$ on $\mathcal{T}_h^1$.

During the adaptation, we use following formula for each triangle K;

$$\alpha_K^{k+1} = max\left(\frac{\alpha_K^k}{1+\kappa*\left(\left(\frac{\eta_K^i}{||\eta^i||_\infty}\right)-0.1\right)^+}, \alpha_{trh}\right), \quad i=1,2$$

where α_{trh} is a threshold parameter and κ is a coefficient chosen to control the rate of decreasing in α, $(u^+) = \max(u, 0)$. Let us give more details on the implementation of this adaptive algorithm which consists of two steps. First, we build an adapted isotropic mesh $\mathcal{T}_h^1$(in the sense of the finite element method, i.e., with respect to the parameter h) with the error indicator η_K^i $(i = 1, 2)$. The adapted mesh is obtained by formally coarsening the initial one in the homogeneous regions and refining it 'close' to the jump set of u in order to 'follow' the edges. Second, we control the function α locally on any element K of $\mathcal{T}_h$. Whenever η_K^i, $(i = 1, 2)$ is calculated and it is more or less large, we have a priory information about the edges. Thus, we may keep the value of α very small in order to approximate correctly the edges in such non-smooth regions. In the complementary regions, where the variations of the intensity are weak, the gradient is low (η_K^i $(i = 1, 2)$ is small). Therefore, we keep α large in order to encourage smoothing.

III. Γ-convergence analysis of the adaptive algorithm

A Γ-convergence study of the adaptive strategy was down in [6] for the optical flow estimation. It was shown that this strategy is equivalent to the adaptive method presented and detailed in [9], [8]. This method approximates, in the Γ-convergence [7] sense, the Mumford-Shah functional. We recall now the results presented in [9]. For a fixed angle $\theta_0 > 0(\theta_0 \leq 60)$, a constant $c \geq 6$, and for $\epsilon > 0$, we set $\mathcal{T}_\epsilon(\Omega) = \mathcal{T}_\epsilon(\Omega; \theta_0; c)$ be the set of all triangulations of Ω whose triangles K have the following characteristics:

- The length of all three edges of K is between ϵ and ϵc.
- The three angles of K are greater than or equal to θ_0.

Let $V_\epsilon(\Omega)$ the set of all continuous functions $u : \Omega \longrightarrow R$ such that u is affine on any triangle K of a triangulation $T \in \mathcal{T}_\epsilon(\Omega)$ and for a given u, $\mathcal{T}_\epsilon(u) \subset \mathcal{T}_\epsilon(\Omega)$ is the set of all triangulations adapted to u,i. e, such that u is piecewise affine on T. They introduce a non-decreasing continuous function $f : [0, +\infty) \longrightarrow [0, +\infty)$ such that:

$$\lim_{t\to 0}\frac{f(t)}{t} = 1, \ \lim f(t) = f_\infty$$

In [9], for any $u \in L^p(\Omega), (p \geq 1)$ and $T \in \mathcal{T}_\epsilon(\Omega)$, the authors introduced the following minimization problem:

$$G_\epsilon(u) = \min_{T\in\mathcal{T}_\epsilon(\Omega)} G_\epsilon(u, T) \tag{9}$$

where

$$G_\epsilon(u,T) = \begin{cases} \sum_{K\in T}|K\cap\Omega|\frac{1}{h_K}f(h_K|\nabla u|^2), & u \in V_\epsilon(\Omega), T \in \mathcal{T}_\epsilon(\Omega) \\ +\infty, & \text{Otherwise.} \end{cases}$$

They proved, as ϵ goes to zero and provided θ_0 is less than some $\Theta > 0$, G_ϵ Γ-converges to the Mumford-Shah functional:

$$G(u) = \begin{cases} \int_\Omega |\nabla u(x)|^2\,dx + f_\infty\mathcal{H}^1(S_u), & u \in L^2(\Omega)\cap GSBV(\Omega) \\ +\infty, & u \in L^2(\Omega)\backslash GSBV(\Omega). \end{cases}$$

where $GSBV(\Omega)$ is the generalized special function of bounded variation (see [11]). It follows from the Γ-convergence to G_ϵ [[9], Theorem 2]:

Theorem 3.1: Let $(u^\epsilon)_{\epsilon>0}$ be a family of functions such that $u^\epsilon \in V_\epsilon(\Omega)$ for all ϵ and

$$\sup_{\epsilon>0} G_\epsilon(u^\epsilon) + ||u^\epsilon||_{L^2(\Omega)} < +\infty \tag{10}$$

Then, there exists $u \in GSBV(\Omega)$ and a subsequence u^{ϵ_j} converging to u a.e. in Ω, such that:

$$G(u) \leq \liminf G_{\epsilon_j}(u^{\epsilon_j}),$$

and, if for each ϵ, u_ϵ is a solution of:

$$\min_v G_\epsilon(v) + \int_\Omega \lambda(x)|v - f|^2 dx, \tag{11}$$

then the limit u solves

$$\min_v G(v) + \int_\Omega \lambda(x)|v - f|^2 dx, \tag{12}$$

and u_{ϵ_j} converges strongly to u.
From convex analysis, we can write:

$$f(t) = \min_{v\in[0,1]} tv + \psi(v)$$

where ψ is the Legendre-Fenchel transform of f. The minimum is achieved for $v = f'(t)$ and therefore, for a given triangulation T_ϵ, the minimization of G_ϵ is then equivalent to minimize the following functional:

$$G'_\epsilon(u, v, T_\epsilon) = \sum_{K\in T_\epsilon} |K\cap\Omega|\frac{1}{h_K}(v_K|\nabla u|^2 + \frac{\psi(v_K)}{h_K}),$$

over all $u \in V_\epsilon(\Omega)$ and $v = (v_K)_{K\in\mathcal{T}_\epsilon}$, piecewise constant on each $K \in T_\epsilon$. For a fixed u, the minimizer over each v is explicitly given by:

$$v_K = f'(h_K|\nabla u|^2) \tag{13}$$

and the optimal u for fixed v solves an elliptic equation. The algorithm of the iterative method used in [9] is then similar of the adaptive strategy presented in this paper and the local choice of α using the error indicator η_K^2 is similar of the choice of v_K in (13) with $v = \alpha$.

IV. Joint image restoration and inpainting

There is typically a trade-off between noise removal and edges preservation because, in some cases, the known portions of the image in $\Omega\backslash D$ are corrupted by noise. The latter will affect the domain D via the available information in ∂D. To overcome this problem, the most practical idea is to simultaneously denoise the available part of the image and fill-in the missing ones.

Starting with a large value of α in the adaptation steps will certainly smooth the input image f in $\Omega\backslash D$ at the first iterations which causes the loss the edges. However, in these known portions, we want to eliminate noise and not edges. Thus, the two parameters α and λ might be controlled adaptively in order to join inpainting and restoration. We assume in this case that the parameter λ is not constant and it depends on the postion of $x \in \Omega\backslash D$. Then, for each element $K \subset \Omega\backslash D$, we have:

$$\begin{aligned}\eta_K^1 &= \alpha_K^{-\frac{1}{2}} h_K ||\lambda_h(u_{\alpha,h} - f_h) + \alpha_h \Delta u_{\alpha,h}||_{L^2(K)} \\ &+ \frac{1}{2} \sum_{e \in E_K} \alpha_e^{-\frac{1}{2}} h_e^{\frac{1}{2}} |||[\alpha_e \nabla u_{\alpha,h} \cdot n_e]||_{L^2(e)}\end{aligned} \tag{14}$$

For $K \subset D$, we have:

$$\begin{aligned}\eta_K^1 &= \alpha_K^{-\frac{1}{2}} h_K ||\alpha_K \Delta u_{\alpha,h}||_{L^2(K)} \\ &+ \frac{1}{2} \sum_{e \in E_K} \alpha_e^{-\frac{1}{2}} h_e^{\frac{1}{2}} |||[\alpha_e \nabla u_{\alpha,h} \cdot n_e]||_{L^2(e)}\end{aligned} \tag{15}$$

where $\alpha_e = \max(\alpha_{K1}, \alpha_{K2})$, K_1 and K_2 being the two elements adjacent to e. In the first residual error indicator, the following quantity

$$E_K = \alpha_K^{-\frac{1}{2}} h_K ||\lambda_h(u_{\alpha,h} - f_h) + \alpha_h \Delta u_{\alpha,h}||_{L^2(K)} \tag{16}$$

acts as a confidence measure locating regions of large errors in the computed solution relatively to to the input noisy image f in $\Omega\backslash D$.

To inapint, we control the diffusion coefficient $\alpha(x)$ in the sub domain D and in the same way as the algorithm II-1. To restore the complementary region $\Omega\backslash D$, we keep $\alpha(x)$ constant and we control the regularization parameter λ by increasing it near the edges to privilege the fidelity part $||\lambda(u-f)||_{L^2(\Omega\backslash D)}$. The update of λ is automatic and locally depending on the position of $x \subset \Omega\backslash D$ by the use of the following formula: For $K \in \Omega\backslash D$;

$$\lambda_K^{(k+1)} = \min\{\lambda_K^k * \left(1 + \kappa * \left(\left(\frac{E_K}{||E||_\infty}\right) - 0.1\right)^+\right), \lambda_{thr}\},$$

where λ_{thr} is a threshold parameter.

V. Adaptive strategy for the complex Ginzburg-Landau equation

This equation was originally developed by Ginzburg & Landau in [12] to phenomenologically describe phase separation and it is given by:

$$-\Delta u + \frac{W'(u)}{\epsilon^2} = 0 \tag{17}$$

where $u : \Omega \longrightarrow [-1, 1]$, ϵ is a small positive parameter and $W(u) = (1 - |u|^2)^2$. It is the Euler Lagrange equation associated to the minimizing of the following energy

$$\frac{1}{2} \int_\Omega |\nabla u|^2 dx + \int_\Omega \frac{W(u)}{2\epsilon^2} dx, \tag{18}$$

This equation was used in several works in image processing probelms [13], [14], [15]. For digital image inpainting purposes, it was developed by H. Grossauer and O. Scherzer in [14]. The key advantage of this model is that its solutions are known to produce effects like vortices and shock-waves of the phase when $\epsilon \longrightarrow 0$ and the solution reveals high contrast in the inpainting domain, which makes it particularly suited for the inpainting task.

The real Ginzburg-Landau equation (17) is appropriate only for two-scale images because the minima of the potential function W are attained in the sphere $|u| = 1$. For gray-scale images, we follow the same methodology of Grossauer and Scherzer in [14]. We rescale the intensity of the input image $f(x)$ to the interval $[-1, 1]$. Then f is identified with the real part of the complex valued function $f_{re} : \Omega \longrightarrow C$ such that:

$$\begin{cases} f = f_{re} + i f_{im}, \text{ where :} \\ f_{re} = \text{the initial damaged image } f_0, \\ f_{im} = \sqrt{1 - f_0^2} \end{cases} \tag{19}$$

By this choice, the complex valued solution u will also have an absolute value equal to 1 but inpainted image (the real part of u) may contain any value from the interval $[-1, 1]$. Thus, for a gray-scale images, we seek to find a minimizer $u_\alpha \in H^1(\Omega, C)$ of the following Ginzburg-Landau type energy:

$$F_\epsilon(u) = \int_\Omega \frac{\alpha(x)}{2} |\nabla u|^2 dx + \int_\Omega \frac{W(u)}{2\epsilon^2} dx + \int_\Omega \frac{\lambda}{2} (u - f)^2 dx, \tag{20}$$

where $H^1(\Omega, C)$ is the Hilbert space of complex functions. A minimizer u_α of F_ϵ satisfies the following Euler-Lagrange equation:

$$\begin{cases} -\nabla.[\alpha(x)\nabla u_\alpha] + \frac{1}{\epsilon^2} u_\alpha (|u|_\alpha^2 - 1) + \lambda(u_\alpha - f) = 0, & \text{in } \Omega, \\ \alpha(x)\partial_n u_\alpha = 0, & \text{on } \partial\Omega. \end{cases} \tag{21}$$

Proposition 2: Let $f \in L^2(\Omega)$ be given with $|f(x)| \leq 1$ a.e. in Ω. The functional (20) admits a unique minimizer u_α in $H^1(\Omega, C)$ with $|u(x)| \leq 1$ a.e. in Ω.

Evolution equation:: As it is often done, to solve problem (21), we transform it into a dynamical scheme as follows:

$$\frac{\partial u_\alpha}{\partial t} - \nabla.[\alpha(x)\nabla u_\alpha] + \frac{W'(u_\alpha)}{\epsilon^2} + \lambda(u_\alpha - f) \quad \text{in } \Omega, \tag{22}$$

with homogeneous Neumann boundary conditions and the initial time condition $u_\alpha(t = 0, x) = f$.

Time discretization:: We use an explicit Euler scheme with respect to the time variable t to approximate $\frac{\partial u_\alpha}{\partial t}$ by $\frac{u_\alpha^{n+1} - u_\alpha^n}{\delta t}$ (where n stands for the iteration time and δt is the time step). We discretize $\nabla \cdot [\alpha(x)\nabla u_\alpha]$ with u_α^{n+1} and the nonlinear term $W'(u_\alpha)$ with u_α^n and u_α^{n+1} as follows

$$W'(u_\alpha^{n+1}) \approx (|u^{n_\alpha}|^2 - 1) u_\alpha^{n+1}$$

More precisely, the time discrete form leads to the following semi-implicit problem: Having u_α^n, find $u_\alpha^{n+1} \in H^1(\Omega)$ such that:

$$\int_\Omega \frac{u_\alpha^{n+1} - u_\alpha^n}{\delta t} \phi dx + \int_\Omega \alpha_h \nabla u_\alpha^{n+1} \nabla \phi dx + \int_\Omega \frac{W'(u_\alpha^{n+1})}{\epsilon^2} \phi dx$$

$$+\int_{\Omega}\lambda(u_{\alpha}^{n+1}-f)\phi dx=0\ \ \forall\phi\in H^{1}(\Omega,C).$$

VI. Numerical examples

In this work, all the PDEs were numerically solved using FreeFem++ [16], a finite element free software. In all examples, the damaged regions are marked with red.

In the first example, the task is to inpaint gaps in a white stripe. We display in Fig. 3 the evolution of the meshes at the iterations 0, 10 and 20. We can see that they are progressively sparsified. The first is the initial mesh $\mathcal{T}_0$ which is regular such that every node corresponds to a pixel in the image. We give in Fig. 4 the damaged image and the results obtained using Harmonic model (2) and our model (4) with adaptation. Harmonic inpainting (middle-hand plots of Fig. 4) is achieving no connection, producing a smooth solution u in D. Contrariwise, We can see the efficiency of the proposed adaptive method (right-hand plots of Fig. 4) and the edges of the stripe were connected sharply.

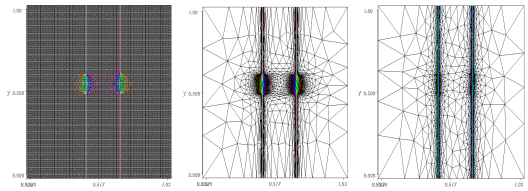

Fig. 3. The mesh at the iterations 1, 10 and 20, respectively.

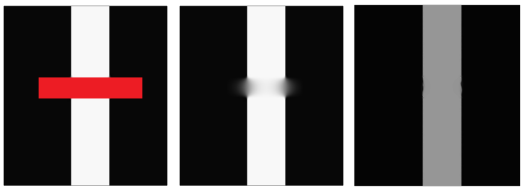

Fig. 4. From left to right: Damaged, Harmonic (2) and model (4) & adaptation images, respectively.

In the second example, we have chosen a gray-scale image (220×220 Pixels) containing edges and jumps. We illustrate in Fig. 5 the damaged image and the results obtained using total variation (middle) and Harmonic model (2) (right). In Fig. 6, we display the inpainted images using the proposed model (4) where the adaptation was made using the error indicators η_K^1 (left) and η_k^2 (middle). For both cases, we initialized the algorithm by a large value of $\alpha=50$ and we performed 20 adaptive iterations for the error indicator η_K^2 and 40 iterations for η_K^1. The right-hand plots of Fig. 6 is the restored image using the Ginzbrg-Landau equation where the adaptation was made using the error indicator η_k^2. We mention that in this case, we took the solution of the Harmonic equation (α is a constant) as an initial guess u_0 in the time discretization.
Increasing the values of α by iteration in the same time with the mesh adaptation allows to obtain sharp edges and less regularization (smoothing) at these locations. We give in Fig. 7 a zoom caption in the damaged region 1 for the different models. We remark that our model gives a comparable result to the one obtained using the Ginzburg-Landau equation.
We present in Fig. 8 the evolution of the meshes for various time iterations (1,5 and 20) where we used η_k^2 as an error indicator. The curve in the right-hand plots of Fig. 9 represents the degrees of freedom as a function of adaptation iterations. It explains how the algorithm works: after some iteration, the number of elements decreases very quickly, then more slowly to improve the sparsification by updating α. We also give in the left-hand plots of Fig. 9the L^2-error between the restored and the exact image as a function of adaptation iterations.
The experiment in Fig. 10 shows the efficiency of the proposed method in a very promising application. The aim is to remove the foreground text in the input image. The text have been successfully removed and the image is well restored.

Fig. 5. From left to right: Damaged image, Total variation and Harmonic model (2) results.

Fig. 6. From left to right: restored images using model (4) & adaptation (error indicator η^1), model (4) & adaptation (error indicator η^2) and Complex Ginzburg-Landau model (22) & adaptation.

Fig. 7. Zoom on region 1: From let to right: TV, Harmonic (2), Harmonic (4) & adaptation (error indicator η^2), Ginzburg-Landau (22) & adaptation and Harmonic (4) & adaptation (error indicator η^1), respectively.

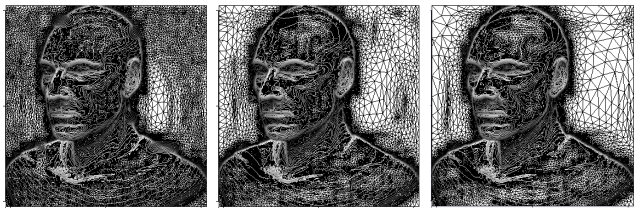

Fig. 8. The mesh at the iterations 1, 2 and 20.

We present in Fig. 11 the result for simultaneous image inpainting and restoration. The input image f is contaminated

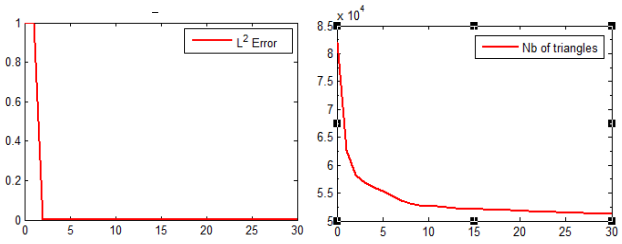

Fig. 9. Left: L^2-error $ER = ||u_\alpha^k - u_{exact}||_2$ as function of adaptation iterations. Right: Number of degrees of freedom as function of adaptation iterations.

Fig. 10. The damaged, mask and restored images, respetively.

by a Gaussian noise in the region $\Omega \backslash D$. We performed 20 adaptive iterations and we display the evolution of the restored image for iterations 5 and 20. In the 5th iteration (middle), the image is smoothed in the know regions. The adaptation processes of λ near the edges in this case allows us to recover discontinuities in $\Omega \backslash D$ (see right-hand plot of Fig. 11).

Fig. 11. From left to right: Damaged and noisy - restored at iteration 5 - restored at iteration 20.

In Fig 12, we tested the behavior of the different methods when the damage region contains a corner. For the harmonic model & adaptation (see the middle-hand plots of Fig 12), we can approximate the corner (but not well achieved!) and the edges are improper contrasted. In the left-hand plots of Fig 12, we display the solution of the complex Ginzburg-Landau equation. First, the complexification allows us to diffuse more than two phases. Second, this model with adaptation allows us to approximate the corner between the homogeneous regions and reveals high contrast, which is the key advantage of this model compared to others and so it makes it particularly suited in this case.

Conclusion

We have investigated an adaptive approach for image inpainting based on a local selection of the different parameters in the models, and on mesh adaptation techniques. We

Fig. 12. From left to right: Damaged and the restored image using Harmonic models (4) & adaptation, and complex Ginzburg-Landau (22) & adaptation, respectively.

started with the formulation of a linear variational models, and detailed its numerical implementation based on the adaptive discretization which approximate in the sense of the Γ-convergence the Mumford-Shah functional. Numerical experiments on different images were performed and showed the efficiency of the proposed method. We can also say that the linear continuous model presented in this work gives the same final result that one might expect by solving a nonlinear one.

References

[1] T. Chan and J. Shen, "Mathematical models for local non-texture inpainting," *SIAM Journal on Applied Mathematics*, vol. 62, no. 2, pp. 1019–1043, 1992.

[2] S. Esedoglu and J. Shen, "Digital image inpainting by Mumford-Shah-Euler model," *European Journal of Applied Mathematics*, vol. 13, pp. 353–370, 2002.

[3] T. Chan and J. Shen, "Non-texture inpainting by curvature-driven diffusions," *J. Visual Comm. Image Rep*, vol. 63, no. 2, pp. 564–592.

[4] M. Kallel, M. Moakher, and A. Theljani, "The cauchy problem for a nonlinear elliptic equation: Nash-game approach and application to image inpainting," *(Submitted)*, .

[5] Z. Belhachmi and F. Hecht, "Control of the effects of regularization on variational optic flow computations," *Journal of Mathematical Imaging and Vision*, vol. 40, no. 1, pp. 1–19, 2011.

[6] Z. Belhachmi and F. Hecht, "An adaptive approach for segmentation and Tv edge-enhacement in the optic flow estimation," *To appear*.

[7] A. Braides, *Gamma-Convergence for Beginners*. In Oxford Lecture Series in Mathematics and its Applications. Oxford University Press, 2002, no. 22.

[8] A. Chambolle and B. Bourdin, "Implementation of an adaptive fnite-element approximation of the mumford-shah functional," *Numer. Math*, 2000.

[9] A. Chambolle and G. D. Maso, "Discrete approximation of the mumford-shah functional in dimension two," *M2AN Math. Model. Numer. Anal*, vol. 33, no. 4, pp. 651–672, 1999.

[10] R. Verfurth, *A Review of A Posteriori Error Estimation and Adaptive Mesh-Refnement Techniques*. Wiely & Teubner, 1996.

[11] L. Ambrosio, N. Fusco, and D. Pallara, *Functions of bounded variation and free discontinuity problems*. Oxford Mathematical Monographs, 200.

[12] L. Landau and V. Ginzburg, "On the theory of superconductivity," *Journal of Experimental and Theoretical Physics (USSR)*, vol. 20, 1950.

[13] Z. Belhachmi and D. Gilliocq-Hirtz, "Coupling parareal and adaptive control in optical flow estimation with application of movie's restauration," *(in prparation)*, .

[14] H. Grossauer and O. Scherzer, "Using the complex ginzburg-landau equation for digital inpainting in 2d and 3d," *Scale Space Methods in Computer Vision, Lecture Notes in Computer Science 2695*, 2003.

[15] G. Aubert and J.-F. Aujol, "Detecting codimension-two objects in an image with ginzburg-landau models," *International Journal of Computer Vision*, vol. 65, no. 1, pp. 29–42, 2005.

[16] F. Hecht, "New development in freefem++," *Journal of Numerical Mathematics*, vol. 20, pp. 251–265, 2002.